iScience

Article

Inferring global exponents in subsampled neural systems

Graphical abstract

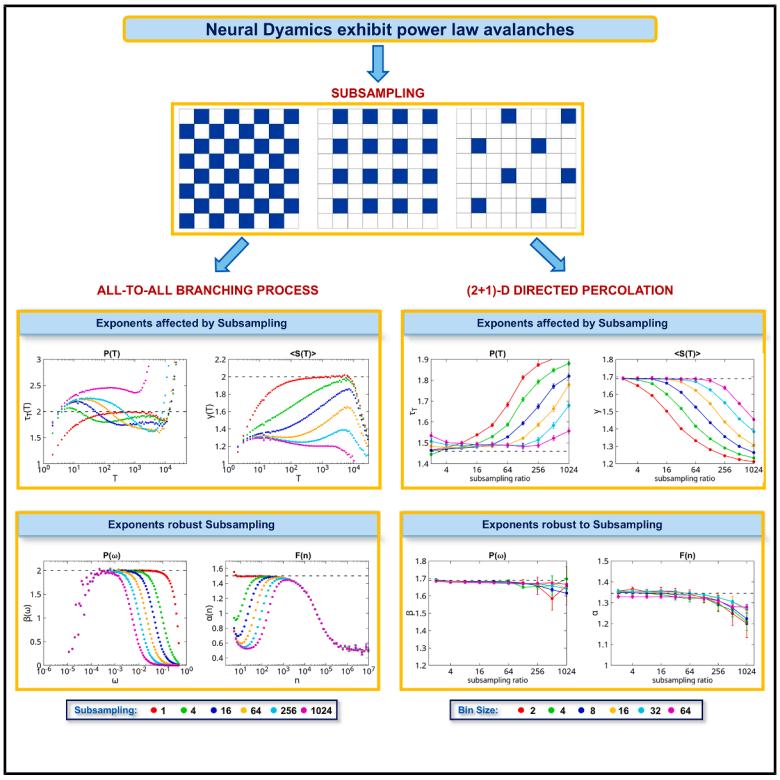

Authors

Davide Conte, Antonio de Candia

Correspondence

davide.conte@unicampania.it (D.C.),
antonio.decandia@unina.it (A.d.C.)

In brief

Natural sciences; Biological sciences; Neural networks

Highlights

- Neural activity exhibits avalanche dynamics with power-law size and duration distributions
- Subsampling alters these distributions and biases estimates of critical exponents
- Exponents governing power spectrum and DFA remain stable under subsampling
- This robustness enables inferring global critical exponents reliably from partial data

Conte & de Candia, 2025, iScience *28*, 113049
August 15, 2025
https://doi.org/10.1016/j.isci.2025.113049

CellPress

iScience

CellPress
OPEN ACCESS

Article

Inferring global exponents in subsampled neural systems

Davide Conte[1,4,5,*] and Antonio de Candia[2,3,4,*]
[1]Department of Mathematics & Physics, University of Campania "Luigi Vanvitelli", viale Lincoln 5, 81100 Caserta, Italy
[2]Dipartimento di Fisica "E. Pancini", Università di Napoli Federico II, Complesso Universitario di Monte Sant'Angelo, via Cintia, 80126 Napoli, Italy
[3]INFN, Sezione di Napoli, Gruppo collegato di Salerno, Fisciano, SA, Italy
[4]These authors contributed equally
[5]Lead contact
*Correspondence: davide.conte@unicampania.it (D.C.), antonio.decandia@unina.it (A.d.C.)
https://doi.org/10.1016/j.isci.2025.113049

SUMMARY

In systems exhibiting avalanche-like activity, critical exponents can provide insights into the mechanisms underlying the observed behavior or on the topology of the connections. However, when only a small fraction of the units composing the system are observed and sampled, the measured exponents may differ significantly from the true ones. In this study, using branching process and (2 + 1)D directed percolation, we show that some of the exponents, namely the ones governing the power spectrum and the detrended fluctuation analysis (DFA) of the system activity, are more robust and are unaffected in some intervals of frequencies by the subsampling. This robustness derives from the preservation of long-time correlations in the subsampled signal, even though large avalanches can be fragmented into smaller ones. These results don't depend on the specific model and may be used therefore to extract in a simple and unbiased way some of the exponents of the unobserved full system.

INTRODUCTION

The evolution of systems observed in Nature is constantly influenced by their response to external perturbations. Numerous studies have demonstrated that many physical systems, despite their macroscopic differences, share similar underlying dynamics. In particular, due to these perturbations, a single event can trigger a cascade of subsequent events, known as an *avalanche*, showing power law distributions of sizes and durations. This behavior, referred to as crackling noise,[1,2] has been observed across a wide range of phenomena, including Barkhausen noise,[3] earthquakes,[4,5] solar flares,[6] biological systems,[7,8] stock markets,[9–11] epidemic spread,[12] and neural networks.[13–15]

An avalanche is typically defined as a chain of consecutive activities occurring above a threshold over an interval of time. Defining $V(t)$ as the time dependent observable, for example the firing rate in neural networks, the interval of time of the avalanche is a consecutive set of time steps such that $V(t) > \Theta$, preceded and followed by two time steps with $V(t) \leq \Theta$. The duration T of an avalanche is defined as the length of the time interval that characterizes it, while the size S of the avalanche is the integral of $V(t) - \Theta$ over the same interval. In the following, we will take the threshold $\Theta = 0$.

In crackling noise phenomena, the sizes and durations of avalanches follow power-law distributions, which is a defining characteristic of this behavior. The probability distribution of the sizes of the avalanches is given by $P(S) \sim S^{-\tau_S}$, that of durations by $P(T) \sim T^{-\tau_T}$, while the average size of the avalanches of given duration is $\langle S \rangle(T) \sim T^{\gamma}$. In most cases, these exponents satisfy the relation[1,16]

$$\frac{\tau_T - 1}{\tau_S - 1} = \gamma, \qquad \text{(Equation 1)}$$

which is generally valid when the system is critical. Relation (1) indeed can be violated when the system is not tuned at criticality, see for example.[17,18]

The autocorrelation function of a stochastic signal $V(t)$ is defined as $C(t', t' + t) = \langle V(t')V(t' + t)\rangle - \langle V(t')\rangle\langle V(t' + t)\rangle$, where the average $\langle \cdots \rangle$ is done over the realizations of the stochastic process. For a stationary process, in which average quantities do not vary over time, all statistical properties are invariant under a global shift of the time origin, so that the autocorrelation function depends only on the time lag t,

$$C(t) = \langle V(t')V(t' + t)\rangle - \langle V(t')\rangle^2,$$

where the average $\langle \cdots \rangle$ can be done over the time t'.

By the Wiener-Khinchin theorem, the power spectrum is defined as the temporal Fourier transform of the autocorrelation function:

$$P(\omega) = \int_0^\infty dt\, C(t)\cos(\omega t).$$

As shown by Kuntz and Sethna,[2] this too follow a power law behavior in crackling noise, e.g., the power spectrum goes as $P(\omega) \sim \omega^{-\beta}$ at low frequencies, while the high-frequency part is typically dominated by white noise. However, for a finite size system, there is a cut-off in the duration of the avalanches, so that the signal $V(t)$ becomes uncorrelated at very long times, and another white noise regime is observed at very low frequencies, so that the exponent β is actually observed in a finite range of frequencies.

As shown in quite general terms in the study by Kuntz et al.,[2] if different avalanches are uncorrelated, then

$$\beta = \gamma. \qquad \text{(Equation 2)}$$

The condition of uncorrelated avalanches is usually well verified when the time separation between avalanches is large, or if the system reaches an absorbing state between different avalanches, so that memory of past activity is lost. The behavior of power spectrum is strictly connected to that of detrended fluctuation analysis (DFA),[19] that considers the standard deviation of the fluctuations of the detrended signal, over varying intervals of time. For a process $V(t)$ in discrete time $t \in \mathbb{N}$, this is defined in the following way: consider an interval of time $t, t+1, \ldots, t+n-1$ of length $\Delta t = n$, and compute the linear function $Y_k = a + bk$ that best fits the given function $V(t+k)$ with $k = 0, \ldots, n-1$. Then compute

$$F(n) = \sqrt{\frac{1}{n}\sum_{k=0}^{n-1}[V(t+k) - Y_k]^2}.$$

Finally, average $F(n)$ over many non-overlapping intervals of time. The function $F(n)$ is strictly related to the power spectrum of the function $V(t)$.[20] If the power spectrum is proportional to $\omega^{-\beta}$ in some interval of the frequencies, then $F(n)$ will be proportional to n^{α} for a corresponding range of n, with $\beta = 2\alpha - 1$.

The previous discussion concerns systems observed in their entirety. However, our knowledge of the system is often limited to a small fraction of it, making it challenging to obtain predictions of the properties of the global system. Different studies[21,22] have shown that subsampling can significantly alter the observed distributions, even when these distributions are scale invariant. Consequently, the critical exponents measured in subsampled data may deviate from those of the fully sampled system, resulting in violations of the scaling relations. In this work, we demonstrate that there exists a frequency (or timescale) range in which the exponents β of the power-spectrum exponent, and α of the DFA, remain invariant with respect to subsampling.

As the exponent γ relating the mean size to the duration instead changes with subsampling, the relation (2) does not hold anymore in the subsampled system. This can be traced back to the fact that, in a subsampled system, subsequent avalanches are not uncorrelated, as they often are successive fragments of a larger avalanche spanning also not sampled regions of the system. While the exponents of avalanche distributions in subsampled systems, e.g., τ_T or γ, are computed taking into account those fragments as separated independent avalanches, when computing the power spectrum or the DFA, one considers the temporal correlations of the signal, regardless of the fact that the signal is broken up in successive segments. Such correlations at long time scales are the same as in the fully sampled signal. We demonstrate this property within two particular models, the branching process (mean field directed percolation) and (2 + 1)D directed percolation. In the first model, the property can also be derived analytically, while in the second it is confirmed by numerical simulations. However, from the discussion aforementioned it is clear that these results are general and do not depend on the model that produced the signal analyzed, being a consequence of the fact that long time correlations are preserved also in the subsampled signal.

This issue has profound implications across various fields. In neural systems, for instance, it is known that the brain operates near a critical state, as this optimizes dynamic range,[23] information transmission, and information capacity.[24] Neural activity is therefore characterized by avalanches as in crackling noise, whose critical exponents carry information on the underlying neural dynamics or topology of the network. Current technologies can record neural avalanches only from a small portion of the cerebral cortex, leading potentially to systematic inconsistencies in the values of the measured exponents and in the scaling relations. Developing robust methods to infer the global critical exponents from such partial data are therefore essential. In this context, accurate prediction of critical exponents is particularly valuable, not only for advancing our theoretical understanding of brain function, but also for potentially serving as a diagnostic tool.

RESULTS

Branching process

The first model we consider is the paradigmatic model of avalanche spreading, that is the branching process. It corresponds to the mean field version of the directed percolation model. We consider a set of N nodes of the network that can be in two states, active and quiescent. Starting from the absorbing state, in which all the nodes are quiescent, we set one node to the active state, to start a new avalanche. Then, at each time step t and for each node that is active at that time, we find the nodes that are activated by it at time $t + 1$. We use an all-to-all connectivity, so that each active node may activate each of the $N - 1$ other nodes with probability σ/N, where σ is the branching parameter. Nodes that are active at time t become quiescent at time $t + 1$, unless some other node has activated them again. If at some time the absorbing state is reached, the avalanche ends, and at the following time another one is started. In the following we consider the critical value $\sigma = 1$ of the branching parameter.

To simulate the subsampling of the system, we consider a subset formed by $N_{\text{sub}} < N$ nodes, and analyze the avalanches observed taking into account only the N_{sub} nodes. We define the subsampling ratio as $f = N/N_{\text{sub}}$, where $f = 1$ means that we observe all the nodes of the system, while larger values correspond to lower density of observed nodes. Due to the all-to-all connectivity, the results are independent of the chosen subset of the nodes, but depend only on the number N_{sub} of nodes

forming the subset. We measure the distributions $P_{\rm sub}(S)$, $P_{\rm sub}(T)$, and the mean size $\langle S\rangle_{\rm sub}(T)$ for different subsampling sizes $N_{\rm sub}$. We have performed 256 independent runs, each simulating a system with $N = 2^{24} \simeq 1.6{\cdot}10^7$ nodes, and the subsampling ratio f was taken between 1 and 1024. Each run produced about $6{\cdot}10^7$ avalanches for a total time steps of about $2{\cdot}10^9$ (each run took about 8 days of CPU time). In (Figure 1) we show the results regarding the distributions of sizes and durations of the avalanches. In panels A, C and E we show, respectively $P_{\rm sub}(S)$, $P_{\rm sub}(T)$ and $\langle S\rangle_{\rm sub}(T)$ for the different subsampling ratios, while in panels B, D and F we show the corresponding logarithmic derivatives. Given a function $f(x) \propto x^{\alpha}$, the logarithmic derivative is defined as $\frac{d\,\log f(x)}{d\,\log x} = \alpha$, so that it gives a measure of the effective exponent governing the function around some value of the variable. A range of values where the logarithmic derivative is nearly constant corresponds to a range where the function can be well approximated by a power law. As can be seen in (Figure 1B), the exponent of the distribution of the sizes in the fully sampled system is equal to $3/2$ in the whole interval of sizes, except near the cut-off of the distribution. For subsampling ratios between 4 and 256, one can see larger and larger deviations for small sizes, that correspond to the first steeper decay of the distribution $P(S)$. (These are called the "hairs" of the distribution in ref.[21]). There remains however a smaller and smaller interval of sizes that display the same exponent $3/2$ of the full system. Only for subsampling ratio 1024 the distribution always displays a larger exponent (a steeper decay).

The distributions of the durations on the other hand have a different behavior. A large deviation from the expected exponent 2 is observed for small durations already in the fully sampled case (red dots in Figure 1D). For subsampled systems, the exponent 2 is never observed for any range of the duration. Instead, the functions have an initial steeper decay (a larger exponent), and then for large durations a range with an exponent smaller than 2. Also the value of the exponent γ, that is related to both the exponents τ_S and τ_T, is different from the expected value 2 for all the intervals of duration, and hovers around the value $\gamma \simeq 1.3$ for example in the case of a subsampling 256. Therefore, we can conclude that, while there is a range of sizes where the exponent τ_S remains stable also for subsampled systems, exponents τ_T and γ have strong deviations that make difficult to infer the values for the global system.

We now show that the exponent governing the power spectrum remains unchanged for a range of frequencies in the case of the subsampled systems. To do this, let N and $V(t)$ be respectively the total number of sites and the number of active sites at time t in the complete lattice, $N_{\rm sub}$ and $V_{\rm sub}(t)$ the corresponding quantities in the "sampled" set of sites, that is a subset ($N_{\rm sub} < N$ and $V_{\rm sub}(t) \leq V(t)$) of the complete lattice. Due to the all-to-all connectivity, at each step only the number $V(t)$ of the active sites depend on the state of the system at time $t-1$, but not the particular subset of sites that is activated. Therefore, the probability that $V_{\rm sub}(t)$ of the sites of the sampled sublattice are activated is the probability of extracting $V_{\rm sub}(t)$ active sites, in $N_{\rm sub}$ random draws without replacement, from a population of N sites that contains exactly $V(t)$ active sites, that is the hypergeometric distribution[25]

$$P[V_{sub}(t)|V(t)] = \frac{\binom{V(t)}{V_{sub}(t)}\binom{N - V(t)}{N_{sub} - V_{sub}(t)}}{\binom{N}{N_{sub}}}. \qquad \text{(Equation 3)}$$

From the distribution (3), given a value of $V(t)$, one can easily compute the conditional expectation values

$$\langle V_{sub}(t)\rangle_{V(t)} = \sum_{V_{\rm sub}(t)} P[V_{\rm sub}(t)|V(t)]V_{\rm sub}(t) = \frac{N_{sub}}{N}\,V(t),$$

$$\langle V_{sub}(t)^2\rangle_{V(t)} = \sum_{V_{\rm sub}(t)} P[V_{\rm sub}(t)|V(t)]V_{\rm sub}(t)^2 = \frac{N_{sub}^2}{N^2}\,V(t)^2 + N_{sub}\frac{V(t)}{N}\left(\frac{N - V(t)}{N}\right)\left(\frac{N - N_{sub}}{N - 1}\right),$$

$$\langle V_{sub}(t)V_{sub}(t')\rangle_{V(t)} = \langle V_{sub}(t)\rangle_{V(t)}\langle V_{sub}(t)\rangle_{V(t)} = \frac{N_{sub}^2}{N^2}\,V(t)V(t') \quad \text{for } t \neq t',$$

where the last equation follows from the fact that the subset of $V(t)$ active sites is extracted randomly at each step. Now, if $P[V(t)]$ is the probability of having $V(t)$ active sites in the complete lattice at time t, and $P[V(t), V(t')]$ the probability of having $V(t)$ and $V(t')$ active sites at times t and t', then the unconditioned expected values of $V_{\rm sub}(t)$, $V_{\rm sub}(t)^2$ and $V_{\rm sub}(t)V_{\rm sub}(t')$ are

$$\langle V_{\rm sub}(t)\rangle = \sum_{V(t)} P[V(t)]\langle V_{sub}(t)\rangle_{V(t)} = \frac{N_{\rm sub}}{N}\langle V(t)\rangle,$$

$$\langle V_{\rm sub}(t)^2\rangle = \sum_{V(t)} P[V(t)]\langle V_{sub}(t)^2\rangle_{V(t)} = \frac{N_{\rm sub}}{N}\left[\left(\frac{N_{\rm sub}}{N} - \frac{N - N_{\rm sub}}{N(N-1)}\right)\langle V(t)^2\rangle + \frac{(N - N_{\rm sub})}{(N-1)}\langle V(t)\rangle\right],$$

$$\langle V_{\rm sub}(t)V_{\rm sub}(t')\rangle = \frac{N_{\rm sub}^2}{N^2}\sum_{V(t),V(t')} P[V(t), V(t')]V(t)V(t') = \frac{N_{\rm sub}^2}{N^2}\langle V(t)V(t')\rangle \quad \text{for } t \neq t',$$

Therefore, the correlation function of $V_{\rm sub}(t)$ is given by

$$C_{\rm sub}(t) = \frac{N_{\rm sub}}{N}\Delta\,\delta_{t,0} + \frac{N_{\rm sub}^2}{N^2}C(t), \qquad \text{(Equation 4)}$$

where $C(t)$ is the correlation function of $V(t)$, and

$$\Delta = \left(\frac{N - N_{\rm sub}}{N - 1}\right)\left[\langle V(t)\rangle - \frac{\langle V(t)^2\rangle}{N}\right].$$

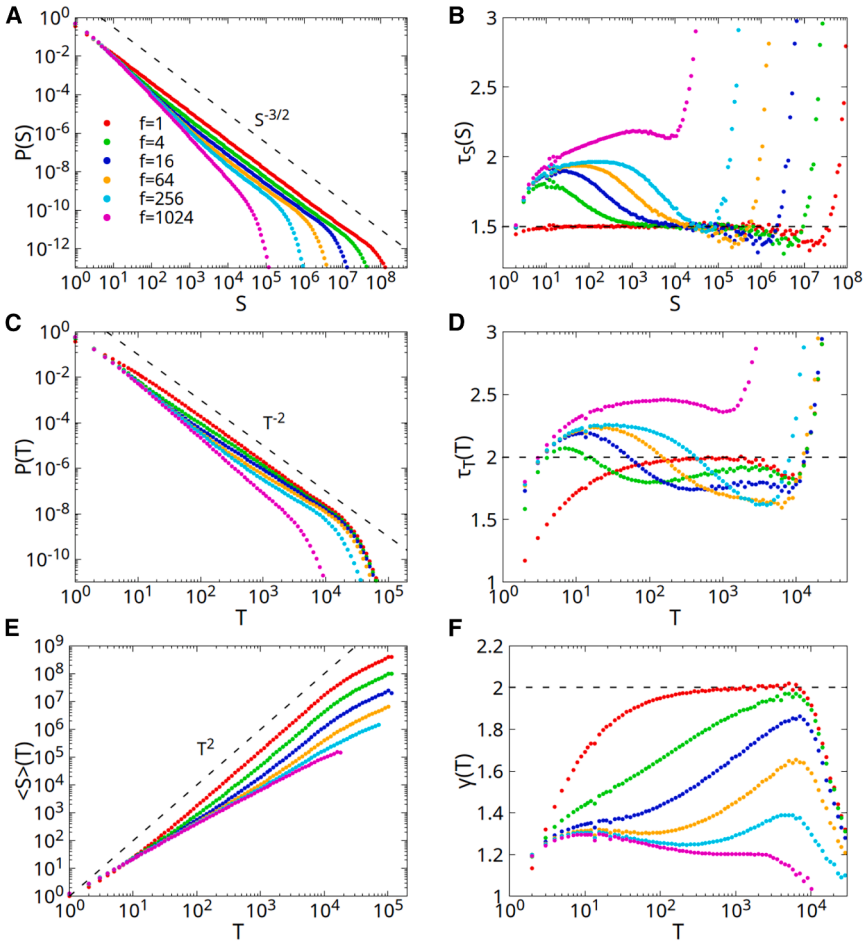

Figure 1. Branching process avalanches distributions

Mean-field branching process on a fully connected network of $N = 2^{24}$ binary sites (active/inactive). To mimic experimental limitations, only a fraction of the active sites is recorded while avalanches extend across the entire lattice. Subsampling ratios $f = N/N_{sub} = 1, 4, 16, 64, 256, 1024$ are shown (color code in legend), with $f = 1$ (red dots) corresponding to the fully sampled case. In all panels, dashed lines mark the theoretical predictions for the fully sampled branching process. In left A, C, E, are shown: size $P(S)$, duration $P(T)$ and mean avalanche size over time $\langle S \rangle (T)$ distributions, respectively. Right panels, B, D and F, show the logarithmic derivatives $\frac{dlogf(x)}{dlogx}$ of the above distributions, which for a pure power law x^{α} yield the exponent α. A plateau in these derivative plots identifies the range over which the data follow a power law. For the fully sampled case $f = 1$, critical exponents $\tau_S = 3/2$, $\tau_T = 2$, and $\gamma = 2$ match mean-field predictions. As f increases, subsampling shifts the cut-offs to smaller S and T and distort the apparent exponents, causing deviations from the fully sampled theory.

Note that for $N_{sub} \ll N$ the coefficient Δ does not depend on the subsampling ratio N/N_{sub}. The power spectrum of the subsampled signal $V_{sub}(t)$ will then be given, due to the Wiener-Khinchin theorem, by

$$P_{sub}(\omega) = \frac{N_{sub}}{N}\Delta + \frac{N_{sub}^2}{N^2}P(\omega). \qquad \text{(Equation 5)}$$

The first term corresponds to a white noise, due to the very fast decorrelation induced by the random choice of the $V_{sub}(t)$ active sites at each step, which is a characteristic of the branching process on a fully connected lattice. Apart from that term, the power spectrum of the number of active sites in the subsampled lattice is exactly proportional to the power spectrum of the full lattice. At the critical point, where $P(\omega) = k\omega^{-\beta}$ with k a constant and $\beta = 2$, the subsampled power spectrum $P_{sub}(\omega)$ will be proportional to $\omega^{-\beta}$ for frequencies $\omega < \omega^*$, and constant for higher frequencies, where $\omega^* = \left(\frac{N_{sub}k}{N\Delta}\right)^{1/\beta}$.

In (Figure 2) we show the results of the simulations of the branching process on the fully connected lattice with $N = 2^{24}$ sites. In panel A we show the power spectrum $P_{sub}(\omega)$ of the number of active sites on the sampled sublattice. The results confirm the expression found before, Equation 5. Note that at very low frequencies there is a white noise plateau, due to the finite size of the lattice and therefore to the cut-off in the distribution of avalanche durations. For times longer than the cut-off (and frequencies lower than the inverse cut-off) the signal we are analyzing is decorrelated because there are no avalanches having such a long duration.

We also consider the DFA of the signal,[19] previously defined. In (Figure 2C) we show the measured functions $F(n)$ and $F_{sub}(n)$ for $V(t)$ and $V_{sub}(t)$. As in the case of the power spectrum, the data always display an interval of frequencies, or interval lengths, where the exponent in the case of subsampled data are equal to that of the fully sampled lattice, see (Figure 2D). This invariance can be therefore exploited to infer exponents of the whole system using only subsampled data. Note that, the larger the subsampling ratio, the smaller the frequency where the high frequency white noise regime sets in. Therefore, for large subsampling ratios, the range where the plateau in the value of the exponent is found may be small, being limited by the two white noise regimes at high and low frequency. However, for larger system sizes, the low frequency regime shifts toward lower frequencies, therefore enlarging the intermediate plateau where the correct exponent is found. This is shown in panels E and F, where the power spectrum and its logarithmic derivatives are shown for the same subsampling ratio $f = 1024$ and for two sizes $N = 2^{24}$ and $N = 2^{28}$. In the larger system the range where the expected exponent $\beta = 2$ is found is correspondingly larger. Data in panel F where filtered to reduce statistical fluctuations

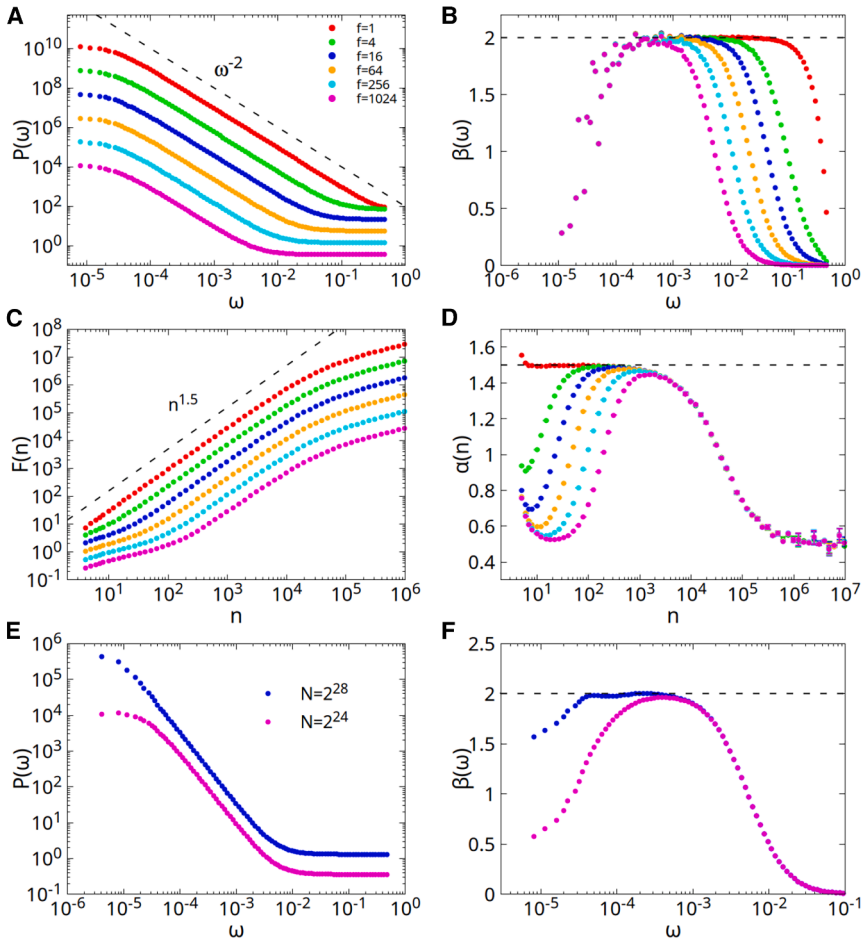

Figure 2. Branching process power spectrum and DFA

(A and C) show power spectrum and detrended fluctuation analysis (DFA) for various subsampling ratios f (case $f = 1$ represents full lattice), with dashed lines indicating theoretical mean-field predictions. Within specific frequency ranges, curves confirm Equation 4 predictions, exhibiting white noise plateaus at very low frequencies due to finite lattice size.

(B and D) display logarithmic derivatives revealing robust exponents under subsampling: $\beta \approx 2$ (power spectrum) and $\alpha \approx 1.5$ (DFA), with deviations only at extreme subsampling ($f = 1024$). Larger subsampling ratios narrow the plateau region between high and low-frequency white noise regimes.

(E and F) demonstrate how larger systems (2^{24} vs. 2^{28}) extend the range where $\beta = 2$ is observed, even with extreme subsampling. For all subsampling ratios, the relation $\beta = 2\alpha - 1$ is consistently maintained. This invariance occurs because both metrics measure temporal autocorrelations of propagating avalanches. While subsampling fragments avalanches (altering their distribution exponents, Figure 1), correlations between fragments remain invariant. The crackling noise relation $\beta = \gamma$ holds only for the full lattice ($\beta = \gamma = 2$ Figures 1F and 2B). Thus, by leveraging the invariance of β, we can estimate critical exponents of avalanche distributions even from subsampled lattices.

at very low frequencies, namely the plotted function is the convolution

$$\tilde{d}(\omega) = \int_{-\infty}^{\infty} \frac{d \ln \omega'}{\sqrt{2\pi\lambda^2}} \exp\left[\frac{(\ln \omega' - \ln \omega)^2}{2\lambda^2}\right] d(\omega'),$$

with $\lambda = 0.5$ and $d(\omega)$ is the function before filtering.

Directed percolation on a (2 + 1)D lattice

In this Section, we consider the directed percolation model on a (2 + 1)D lattice, that corresponds to a branching process not on a fully connected lattice but on a 2D lattice. While the critical exponents in this case are different from the mean field values found in the previous Section, we again find that power spectrum and detrended fluctuation exponents remain invariant in the case of subsampling for a range of frequencies or interval lengths.

The directed percolation model on a (2 + 1)D lattice is defined as follows. Consider a 2D square lattice, where each site can be activated or quiescent. Each site that is activated at time t may activate at time $t + 1$ each of its four neighbors with probability p. A node that is active at time t becomes quiescent at time $t + 1$, unless some of its neighbors has activated it again. As in the case of the branching process studied in the previous Section, if all the sites are quiescent, we start a new avalanche selecting a site at random and activating it. We simulate the system at the critical value of the probability, $p_c \simeq 0.28729$,[26] and for $L = 1024$, $N = L^2 \simeq 10^6$ sites, until 10^7 avalanches have been observed (about 14 days of CPU time).

To assess the effects of subsampling also in the case of (2 + 1) D directed percolation, we take a subset of the sites of the lattice as done in the previous case, and consider the number $V_{\text{sub}}(t) \leq V(t)$ of sites active at time t. In (Figure 3) we show the criterion used to choose the subset of sites for subsampling ratios 2, 4, and 8. In a similar way sites are selected for higher ratios. We have considered ratios between 1 and 1024.

To check also the dependence on temporal binning, we also use different temporal bin sizes. Specifically, for a bin size $w = 2, 4, \ldots$, we define a new function $V_{\text{sub},w}(t)$, with $t \in \mathbb{N}$, as the sum of $V_{\text{sub}}(t')$ for $t' = wt, wt + 1 \ldots w(t + 1) - 1$, and then compute avalanche distributions and power spectrum for this new function. Note that, in the subsampled case, it is essential to choose a temporal bin $w = 2$ or larger. This is because, for the subsampling criterion chosen, sampled (blue) sites can be active only every other time step, so that with $w = 1$ every avalanche would be divided into pieces of duration one step. We considered temporal bins between $w = 2$ and $w = 64$. Given

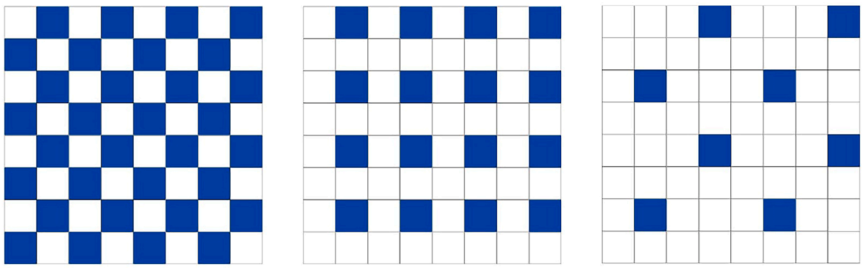

Figure 3. Subsampling criterion in directed percolation

Blue sites are the ones selected for subsampling, for ratios $N/N_{sub} = 2, 4, 8$. In a similar way sites are selected for higher ratios.

the number $V(t)$ or $V_{sub}(t)$ of active sites as a function of time, consecutive intervals with $V(t) > 0$ or $V_{sub}(t) > 0$ correspond to avalanches. In (Figure 4) we show the distributions of sizes, durations, mean size versus duration, and the power spectrum for different subsampling ratios. Each of the distributions exhibits a power-law behavior in a large range, and we extract exponents from a least squares fit in that range, excluding the cut-off due to the finite size of the lattice. In the case of the fully sampled lattice, we obtained the following exponents: $\tau_S = 1.27 \pm 0.03$, $\tau_T = 1.46 \pm 0.01$, $\gamma = 1.69 \pm 0.02$, $\beta = 1.70 \pm 0.01$, consistent with those found in the literature,[27] and satisfying the scaling relations of crackling noise (1) and (2). As in the previous case, by applying subsampling, we expect variations in the probability distributions and, consequently, in the respective critical exponents. The effect of subsampling is to fragment a single avalanche into smaller avalanches with reduced size and duration, thus leading to an increase of the exponents for the probability distributions of sizes and durations. This is shown in Figures 6A and 6B, that reports the exponents of the avalanche distributions as a function of the sampling size, for different temporal binnings. As shown in (Figure 6C), the resulting effect of subsampling on the mean size $\langle S \rangle_{sub}(T)$ as a function of duration, is to progressively reduce the exponent as the sampling size decreases, as already observed in the case of the mean field branching process.

As already observed in,[28] the effects of subsampling can be reduced by increasing the width of temporal bins, so that different fragments of the same avalanche are reconnected again. Therefore, the values of the exponents for the fully sampled system tend to be recovered. This is confirmed by our data, where exponents for larger temporal binning remain stable up to higher values of the subsampling ratios.

In (Figure 6D), we show the exponent β of power spectrum decay as a function of subsampling, for different temporal binning. While we have seen that the exponent γ varies under sampling procedures, as shown in (Figure 6C), the exponent β of the power spectrum remains unchanged, as in the case of the branching process. This is because the power spectrum is the Fourier transform of the temporal autocorrelation function between sites within the same avalanche. Although sampling fragments the avalanche into smaller ones, these fragments are not independent but correlated, as they still belong to the same avalanche propagating through the lattice. On one hand, this leads to the violation of the relationship (2), which holds only in the case of uncorrelated avalanches.[2] On the other hand, the exponent β remains unchanged under subsampling, while γ varies, as shown in the inset of (Figure 6D).

The relation between the correlation function of $V_{sub}(t)$ and that of $V(t)$ cannot be evaluated explicitly as in the case of the mean field branching process. However, the form of the power spectrum shows that the correlation function, which is its Fourier antitransform due to Wiener-Khinchin theorem, with respect to Equation 4 generalizes to

$$C_{sub}(t) = \frac{N_{sub}}{N}\Delta(t) + \frac{N_{sub}^2}{N^2}C(t),$$

where $\Delta(t)$ does not depend on $\frac{N_{sub}}{N}$ if $N_{sub} \ll N$, and decays in a short time. It represents the excess probability (with respect to a random choice of sites) that the avalanche at time t overlaps with the same sites of the sampled set as those at time 0. Therefore, the power spectrum in the subsampled case will exhibit two different behaviors: at low frequencies it will be given by $\frac{N_{sub}^2}{N^2}$ times the power spectrum of the fully sampled case. At high frequencies on the other hand, it will go as the Fourier transform of $\Delta(t)$. The plots of (Figure 4D) confirm this prediction. While at low frequencies the spectra all follow a power law with exponent $\beta \simeq 1.7$, at high frequency on the other hand they follow a different power law, with an exponent $\beta_h \simeq 0.6$.

Consistent with previous findings for the branching process, the DFA also exhibits power-law scaling across varying sampling ratios, as illustrated in (Figure 5A). Notably, the observation of a distinct critical exponent β_h for the power spectrum is similarly observed in the DFA: as sampling density increases, a new linear trend emerges for small values of n, with an exponent around 0.8. This result aligns with the power spectrum, as the two exponents are connected through the scaling relation $\beta = 2\alpha - 1$. (Figure 5B) further demonstrates that the exponent α remains approximately invariant across different sampling ratios and temporal binning, consistently satisfying the previously stated scaling relation and the results observed for the branching model.

DISCUSSION

Inferring global critical exponents in systems like neural networks has been a long-standing challenge. Since the seminal work of Beggs and Plenz,[13] it has been hypothesized that the critical exponents of neural avalanches would align with those of the branching process (BP). However, recent advances in technology and research have revealed the existence of critical exponents that differ from those of the BP universality class, suggesting the possibility of multiple universality classes in neural networks.[29–33] Naturally developing cultures show avalanche statistics consistent with those of a mean-field

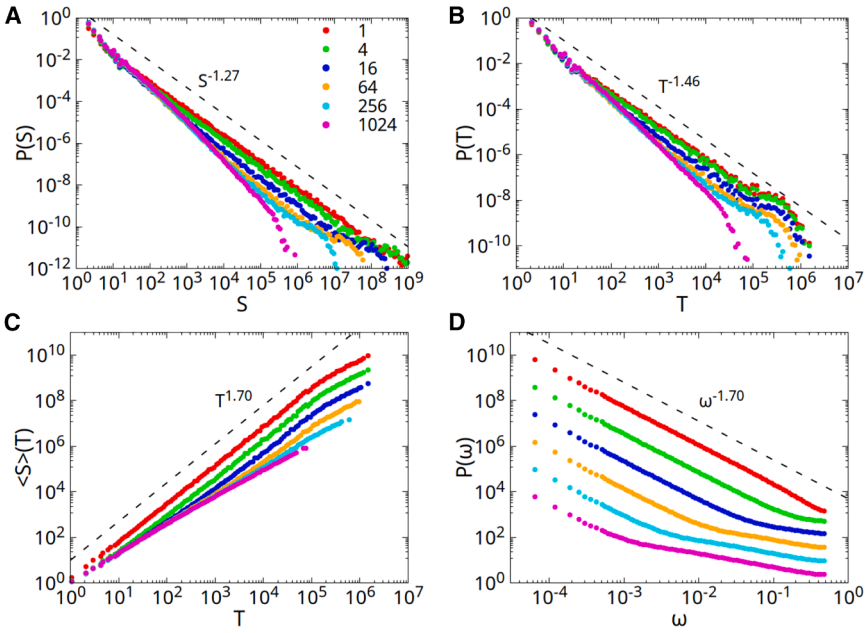

Figure 4. Directed Percolation avalanches distributions and power spectrum

Avalanche distributions and power spectrum for (2 + 1)D Directed Percolation with $N = 1024 \times 1024$ binary sites. Each panel reports the observable of interest. (A): avalanche-size distribution $P(S)$. (B): avalanche-duration distribution $P(T)$. (C) mean avalanche size $\langle S \rangle (T)$ over time. (D): power spectrum $P(\omega)$. All distributions are computed for different spatial subsampling ratios $f = N/N_{sub} = 1$ (full lattice), 4, 16, 64, 256, 1024 and temporal bin width $\omega = 2$, essential to recover the correct avalanche propagation dynamics in the subsampled lattices. Dashed lines represent theoretical curves with the corresponding critical exponents. These differ from those of the branching process, and the numerical results obtained for the full lattice recover the theoretical predictions.[27]

branching process, while cultures grown in the presence of folic acid metabolites appear to be in a distinct universality class with significantly different critical exponents, pointing to a leading role of network topology in shaping avalanche dynamics.[34] Moreover, spontaneous activation in neural circuits may cause otherwise independent avalanches to merge, changing the universality class from directed to undirected percolation.[35]

Given that studies on neural avalanches are typically based on sampled portions of the system, accounting for subsampling effects is crucial, if one wants to accurately estimate critical exponents to identify the universality class to which the system belongs. Previous work by Levina and Priesemann[21] has shown that subsampling can distort avalanche distributions, potentially leading to inaccurate predictions of global critical exponents.

In this study, using two stochastic models, the branching process and (2 + 1)D directed percolation, we have demonstrated that the exponents β of power spectrum and α of DFA are robust with respect to subsampling. Given that these exponents are related to the exponents characterizing the avalanche distributions,[2,36] they can be used to predict the latter when only subsampled data are available.

The underlying reason for this robustness is that the long-time correlations in the activity persist under subsampling: although a single large avalanche may be fragmented into multiple smaller ones, these pieces still form a correlated chain in time. Consequently, the low-frequency region of the power spectrum and the long-range correlations detected by DFA remain approximately unchanged. In contrast, exponents of avalanche-size or avalanche-duration distributions, such as τ_T or γ, treat those fragments as independent events and are therefore strongly affected by subsampling, leading to the violation of the crackling noise relation $\beta = \gamma$, which presupposes uncorrelated avalanches.

Therefore, even when dealing with subsampled systems, as is inevitable in experimental settings, we can estimate the exponent β (or α) and, by exploiting its invariance under subsampling, infer the true avalanche distribution exponents of the full system, relying on the validity of the crackling noise scaling relations in this regime.

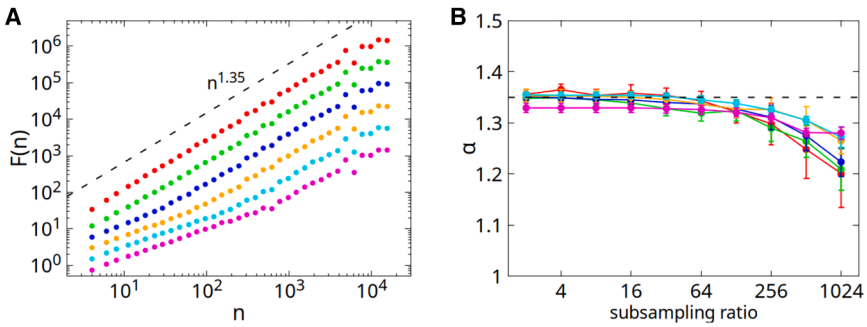

Figure 5. Directed Percolation DFA

(A): detrended fluctuation analysis of the subsampled active sites for different subsampling ratios and bin size $w = 2$. (B): critical exponent α, remains approximately invariant during subsampling procedures, confirming, within error margins, the relationship with the β exponent of the power spectrum $\beta = 2\alpha - 1$.

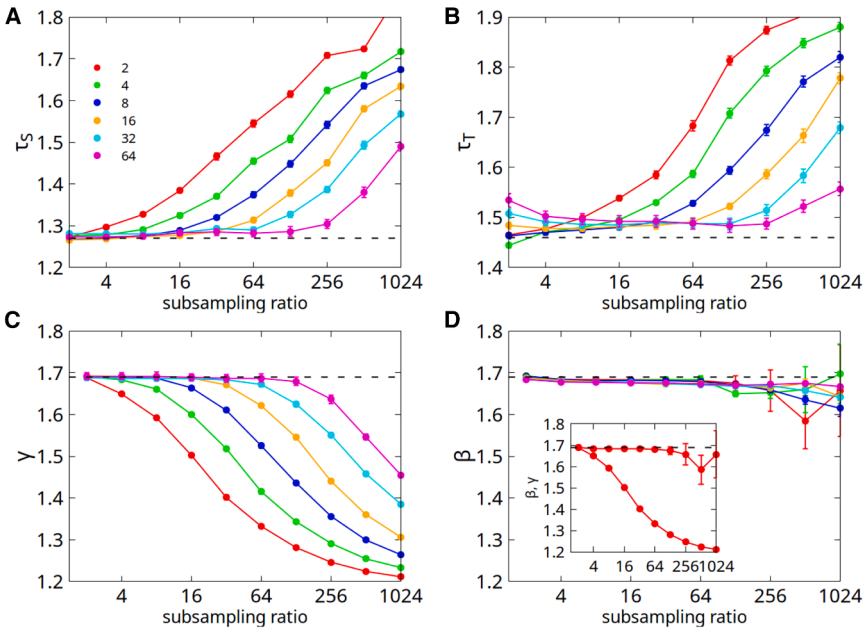

Figure 6. Directed Percolation critical exponents

Figure shows critical exponents τ_S, τ_T, γ and β, extracted with a least squares fit across different subsampling ratios (1–1024, x axis) and temporal binning (2–64, color-coded in legend). In (A and B), we observe that for the exponents τ_S and τ_T of $P_{\text{sub}}(S)$ and $P_{\text{sub}}(T)$, the effect of subsampling results in an increase in the value of the critical exponent, due to the fragmentation of large avalanches into smaller ones. In (C), the exponent γ of $\langle S \rangle_{\text{sub}}(T)$ instead decreases with subsampling. As observed in,[28] increasing the temporal binning allows the global value of the exponent to be recovered. On the other hand, in (D), the exponent β of the power spectrum remains nearly unchanged under subsampling, and for any value of the temporal binning. Inset of (D): Comparison between the exponent of the power spectrum β, and that of the average avalanche size γ, as a function of the subsampling ratio, for a bin size $w = 2$. The two exponents coincide within errors for the case of the complete lattice, both close to 1.7, but as the number of sampled sites decreases, the discrepancy between them increases. Specifically, β remains nearly unchanged across subsampling procedures, while γ decreases. By leveraging the invariance of the β (or α) exponent under subsampling, one can estimate the γ exponent of the full lattice, where the scaling relation $\beta = \gamma$ holds.

Although we have demonstrated these findings for two specific models, the preservation of long-range temporal correlations in partially observed avalanche processes suggests that this effect is not confined to those models alone. Critical exponents may indeed differ for other network topologies, or under different dynamical processes, but the arguments about fragmentation of avalanches versus preserved time correlations apply quite broadly.

Finally, it is worth emphasizing that the invariance of the spectral exponent β (or DFA α) under subsampling is not unique to neuronal avalanches; it simply reflects the persistence of long-range temporal correlations that characterize crackling noise processes. The same models discussed here, branching process and directed percolation, are routinely used to describe this wider family of systems. For this reason, we expect that the method proposed in this work can be applied well beyond neural systems, as subsampling represents a common limitation in many experimental contexts. The same open questions identified in the context of neuronal systems, for example, the potential coexistence of distinct universality classes indicated by varying critical exponents, also emerge in other systems, like Barkhausen noise or material failure, as shown in.[37–39] Obtaining unbiased, reliable estimates of avalanche exponents is a demanding yet essential task in all this family of systems. Our proposed solution, based on the power spectrum, is strengthened by the study of *Travesset* et al.[40] on Barkhausen noise. While not addressing the issue of subsampling, they show that power spectrum is a robust indicator of the universality class.

In the case of the brain, accurate predictions of these exponents could be crucial for identifying variations in the neural activity or in the network topology and, therefore, neurological disorders or pathologies. Achieving this goal is complicated by incomplete and often noisy experimental data, a constraint that theory must necessarily confront. Encouragingly, recent studies are making significant progress in this field, with several demonstrating that the power spectrum can serve as a powerful tool for investigating neural activity.[41–43] Together, these studies demonstrate that the spectral methods advocated here already yield reliable exponents in real neural data, lending practical support to our theoretical framework.

Moving forward, our goal is to extend the findings from this study, demonstrated for the branching process and directed percolation, to more realistic models, ultimately contributing to a deeper understanding of criticality in crackling noise.

Limitations of the study

Our findings rely on analyses performed on two critical models, namely the branching process and (2 + 1)D directed percolation, which are widely employed in theoretical studies of neuronal networks but omit key features inherent to real cortical circuits, including inhibitory interactions, synaptic plasticity, and long-range or heterogeneous connectivity. Although our results demonstrate general principles expected to be robust across different model choices, validation using more biologically realistic and structurally detailed models remains essential.

Our analysis primarily focused on the scaling relation $\beta = \gamma$, demonstrating that the invariance of the power spectrum exponent β can serve as a powerful predictive tool for estimating the global exponent γ from subsampled systems. However, additional studies examining the alternative scaling relation $\gamma = \frac{\tau_T - 1}{\tau_S - 1}$ under subsampling conditions could further strengthen and broaden the applicability of our theoretical framework.

The subsampling method implemented in this study was explicitly detailed; nevertheless, assessing the robustness of

our results under alternative sampling topologies, closer to experimental recording conditions, would be informative.

Ultimately, the theoretical predictions presented here must be validated through high-quality *in vivo* or *in vitro* datasets. Experimental recordings inevitably include instrumental noise, non-stationarities, and biological variability, which may introduce deviations from the idealized scaling behaviors reported, thus highlighting critical areas for future refinement and experimental verification.

RESOURCE AVAILABILITY

Lead contact

Requests for further information and resources should be directed to and will be fulfilled by the lead contact, Davide Conte, (davide.conte@unicampania.it).

Materials availability

This study did not generate new unique reagents.

Data and code availability

- Original codes used in this study are publicly available on https://github.com/decandia/subsampling.
- Any additional information required to reanalyze the data reported in this paper is available from the lead contact upon request.

ACKNOWLEDGMENTS

We acknowledge the use of the LXGRIV cluster of computers, at the Naples Section of INFN (Italian Institute of Nuclear Physics).

We acknowledge funding from INFN, project "COBRA "COmputer Based RNA Analysis and prediction" nell'ambito dell'avviso pubblico relativo al bando a cascata, D.R. n. 750 del 28/02/2024 dell'Università degli Studi di Bari, per lo spoke 7 "BIOCOMPUTING" del progetto PNRR CN00000041 "National Center for Gene Therapy and Drugs based on RNA Technology", Missione 4, Componente 2, Investimento 1.4, finanziato dall'Unione europea—NextGenerationEU—CUP H93C22000430007".

AUTHOR CONTRIBUTIONS

Conceptualization, D.C. and A.d.C.; methodology, D.C. and A.d.C.; simulations, D.C. and A.d.C.; data analysis, D.C. and A.d.C.; writing – original draft, D.C. and A.d.C.; writing – review and editing, D.C. and A.d.C.

DECLARATION OF INTERESTS

The authors declare no competing interests.

STAR★METHODS

Detailed methods are provided in the online version of this paper and include the following:

- KEY RESOURCES TABLE
- METHOD DETAILS
  - Branching Process
  - (2+1)D directed percolation
- QUANTIFICATION AND STATISTICAL ANALYSIS

Received: November 28, 2024
Revised: April 17, 2025
Accepted: June 30, 2025
Published: July 3, 2025

REFERENCES

1. Sethna, J.P., Dahmen, K.A., and Myers, C.R. (2001). Crackling noise. Nature *410*, 242–250. https://doi.org/10.1038/35065675.
2. Kuntz, M.C., and Sethna, J.P. (2000). Noise in disordered systems: The power spectrum and dynamic exponents in avalanche models. Phys. Rev. B *62*, 11699–11708. https://doi.org/10.1103/PhysRevB.62.11699.
3. Cote, P.J., and Meisel, L.V. (1991). Self-organized criticality and the barkhausen effect. Phys. Rev. Lett. *67*, 1334–1337. https://doi.org/10.1103/PhysRevLett.67.1334.
4. Bak, P., and Tang, C. (1989). Earthquakes as a self-organized critical phenomenon. J. Geophys. Res. Solid Earth *94*, 15635–15637. https://doi.org/10.1029/JB094iB11p15635.
5. Olami, Z., Feder, H., and Christensen, K. (1992). Self-organized criticality in a continuous, non-conservative cellular automaton modeling earthquakes. Phys. Rev. Lett. *68*, 1244–1247. https://doi.org/10.1103/PhysRevLett.68.1244.
6. Lu, E.T., and Hamilton, R.J. (1991). Avalanches and the distribution of solar flares. Astrophys. J. *380*, L89–L92. https://doi.org/10.1086/186180.
7. Mora, T., and Bialek, W. (2011). Are biological systems poised at criticality? J. Stat. Phys. *144*, 268–302. https://doi.org/10.1007/s10955-011-0229-4.
8. Nykter, M., Price, N.D., Aldana, M., Ramsey, S.A., Kauffman, S.A., Hood, L.E., Yli-Harja, O., and Shmulevich, I. (2008). Gene expression dynamics in the macrophage exhibit criticality. Proc. Natl. Acad. Sci. USA *105*, 1897–1900. https://doi.org/10.1073/pnas.0711525105.
9. Bak, P., Chen, K., Scheinkman, J., and Woodford, M. (1993). Aggregate fluctuations from independent sectoral shocks: Self-organized criticality in a model of production and inventory dynamics. Ric. Econ. *47*, 3–30. https://doi.org/10.1016/0035-5054(93)90023-V.
10. Tang, L.H., and Tian, G.S. (1999). Reaction–diffusion–branching models of stock price fluctuations. Physica A *264*, 543–550. https://doi.org/10.1016/S0378-4371(98)00549-4.
11. Sornette, D. (2003). Critical market crashes. Phys. Rep. *378*, 1–98. https://doi.org/10.1016/S0370-1573(02)00634-8.
12. Grassberger, P. (1983). On the critical behavior of the general epidemic process and dynamical percolation. Math. Biosci. *63*, 157–172. https://doi.org/10.1016/0025-5564(82)90036-0.
13. Beggs, J.M., and Plenz, D. (2003). Neuronal avalanches in neocortical circuits. J. Neurosci. *23*, 11167–11177. https://doi.org/10.1523/JNEUROSCI.23-35-11167.2003.
14. Shriki, O., Alstott, J., Carver, F., Holroyd, T., Henson, R.N.A., Smith, M.L., Coppola, R., Bullmore, E., and Plenz, D. (2013). Neuronal avalanches in the resting meg of the human brain. J. Neurosci. *33*, 7079–7090. https://doi.org/10.1523/JNEUROSCI.4286-12.2013.
15. Petermann, T., Thiagarajan, T.C., Lebedev, M.A., Nicolelis, M.A.L., Chialvo, D.R., and Plenz, D. (2009). Spontaneous cortical activity in awake monkeys composed of neuronal avalanches. Proc. Natl. Acad. Sci. USA *106*, 15921–15926. https://doi.org/10.1073/pnas.0904089106.
16. Scarpetta, S., Apicella, I., Minati, L., and de Candia, A. (2018). Hysteresis, neural avalanches, and critical behavior near a first-order transition of a spiking neural network. Phys. Rev. E *97*, 062305. https://doi.org/10.1103/PhysRevE.97.062305.
17. Touboul, J., and Destexhe, A. (2017). Power-law statistics and universal scaling in the absence of criticality. Phys. Rev. E *95*, 012413. https://doi.org/10.1103/PhysRevE.95.012413.
18. Ma, Z., Turrigiano, G.G., Wessel, R., and Hengen, K.B. (2019). Cortical circuit dynamics are homeostatically tuned to criticality *in vivo*. Neuron *104*, 655–664.e4. https://doi.org/10.1016/j.neuron.2019.08.031.
19. Peng, C.K., Havlin, S., Stanley, H.E., and Goldberger, A.L. (1995). Quantification of scaling exponents and crossover phenomena in non-stationary heartbeat time series. Chaos *5*, 82–87. https://doi.org/10.1063/1.166141.

20. Heneghan, C., McDarby, G., and O'Regan, S. (2000). Establishing the relation between detrended fluctuation analysis and power spectral density for stochastic processes. Phys. Rev. *62*, 6103–6110. https://doi.org/10.1103/PhysRevE.62.6103.

21. Levina, A., and Priesemann, V. (2017). Subsampling scaling. Nat. Commun. *8*, 15140. https://doi.org/10.1038/ncomms15140.

22. Carvalho, T.T.A., Ribeiro, T.L., Prado, C., and Copelli, M. (2021). Subsampled directed-percolation models explain scaling relations experimentally observed in the brain. Front. Neural Circ. *14*, 576727. https://doi.org/10.3389/fncir.2020.576727.

23. Kinouchi, O., and Copelli, M. (2006). Optimal dynamical range of excitable networks at criticality. Nat. Phys. *2*, 348–351. https://doi.org/10.1038/nphys289.

24. Shew, W.L., Yang, H., Yu, S., Roy, R., and Plenz, D. (2011). Information capacity and transmission are maximized in balanced cortical networks with neuronal avalanches. J. Neurosci. *31*, 55–63. https://doi.org/10.1523/JNEUROSCI.4637-10.2011.

25. Johnson, N.L., Kotz, S., and Kemp, A.W. (1992). Univariate Discrete Distributions, 2 ed.1992 (Wiley).

26. Grassberger, P. (1989). Directed percolation in (2+1) dimensions. J. Phys. A: Math. Gen. *22*, 3673–3679. https://doi.org/10.1088/0305-4470/22/17/032.

27. Muñoz, M.A., Dickman, R., Vespignani, A., and Zapperi, S. (1999). Avalanche and spreading exponents in systems with absorbing states. Phys. Rev. E *59*, 6175–6179. https://doi.org/10.1103/PhysRevE.59.6175.

28. Srinivasan, K., Ribeiro, T.L., Kells, P., and Plenz, D. (2024). The recovery of parabolic avalanches in spatially subsampled neuronal networks at criticality. Sci. Rep. *14*, 19329. https://doi.org/10.1038/s41598-024-70014-4.

29. Apicella, I., Scarpetta, S., de Arcangelis, L., Sarracino, A., and de Candia, A. (2022). Power spectrum and critical exponents in the 2d stochastic wilson–cowan model. Sci. Rep. *12*, 21870. https://doi.org/10.1038/s41598-022-26392-8.

30. Shew, W.L., Clawson, W.P., Pobst, J., Karimipanah, Y., Wright, N.C., and Wessel, R. (2015). Adaptation to sensory input tunes visual cortex to criticality. Nat. Phys. *11*, 659–663. https://doi.org/10.1038/nphys3370.

31. Ribeiro, T.L., Copelli, M., Caixeta, F., Belchior, H., Chialvo, D.R., Nicolelis, M.A.L., and Ribeiro, S. (2010). Spike avalanches exhibit universal dynamics across the sleep–wake cycle. PLoS One *5*, e14129. https://doi.org/10.1371/journal.pone.0014129.

32. Palva, J.M., Zhigalov, A., Hirvonen, J., Korhonen, O., Linkenkaer-Hansen, K., and Palva, S. (2013). Neuronal long-range temporal correlations and avalanche dynamics are correlated with behavioral scaling laws. Proc. Natl. Acad. Sci. USA *110*, 3585–3590. https://doi.org/10.1073/pnas.1216855110.

33. Fontenele, A.J., de Vasconcelos, N.A.P., Feliciano, T., Aguiar, L.A.A., Soares-Cunha, C., Coimbra, B., Dalla Porta, L., Ribeiro, S., Rodrigues, A.J., Sousa, N., et al. (2019). Criticality between cortical states. Phys. Rev. Lett. *122*, 208101. https://doi.org/10.1103/PhysRevLett.122.208101.

34. Yaghoubi, M., de Graaf, T., Orlandi, J.G., Girotto, F., Colicos, M.A., and Davidsen, J. (2018). Neuronal avalanche dynamics indicates different universality classes in neuronal cultures. Sci. Rep. *8*, 3417. https://doi.org/10.1038/s41598-018-21730-1.

35. Korchinski, D.J., Orlandi, J.G., Son, S.W., and Davidsen, J. (2021). Criticality in spreading processes without timescale separation and the critical brain hypothesis. Phys. Rev. X *11*, 021059. https://doi.org/10.1103/PhysRevX.11.021059.

36. Jo, H.H., Birhanu, T., and Masuda, N. (2024). Temporal scaling theory for bursty time series with clusters of arbitrarily many events. Chaos *34*, 083110. https://doi.org/10.1063/5.0219561.

37. Durin, G., and Zapperi, S. (2000). Universality and size effects in the barkhausen noise. J. Appl. Phys. *87*, 7031–7033. https://doi.org/10.1063/1.372921.

38. Bohn, F., Durin, G., Correa, M.A., Machado, N.R., Della Pace, R.D., Chesman, C., and Sommer, R.L. (2018). Playing with universality classes of barkhausen avalanches. Sci. Rep. *8*, 11294. https://doi.org/10.1038/s41598-018-29576-3.

39. Mayya, A., Barés, J., Jagla, E.A., Bonamy, D., and Rosso, A. (2024). Percolation versus depinning transition: The inherent role of damage hardening during quasibrittle failure. Phys. Rev. E *110*, 035003. https://doi.org/10.1103/PhysRevE.110.035003.

40. Travesset, A., White, R.A., and Dahmen, K.A. (2002). Crackling noise, power spectra, and disorder-induced critical scaling. Phys. Rev. B *66*, 024430. https://doi.org/10.1103/PhysRevB.66.024430.

41. Donoghue, T., Haller, M., Peterson, E.J., Varma, P., Sebastian, P., Gao, R., Noto, T., Lara, A.H., Wallis, J.D., Knight, R.T., et al. (2020). Parameterizing neural power spectra into periodic and aperiodic components. Nat. Neurosci. *23*, 1655–1665. https://doi.org/10.1038/s41593-020-00744-x.

42. Dehghani, N., Bédard, C., Cash, S.S., Halgren, E., and Destexhe, A. (2010). Comparative power spectral analysis of simultaneous electroencephalographic and magnetoencephalographic recordings in humans suggests non-resistive extracellular media. J. Comput. Neurosci. *29*, 405–421. https://doi.org/10.1007/s10827-010-0263-2.

43. He, B.J. (2014). Scale-free brain activity: past, present, and future. Trends Cogn. Sci. *18*, 480–487. https://doi.org/10.1016/j.tics.2014.04.003.

STAR★METHODS

KEY RESOURCES TABLE

REAGENT or RESOURCE	SOURCE	IDENTIFIER
Deposited data		
Code to reproduce data	This paper	https://github.com/decandia/subsampling
Software and algorithms		
C++	This paper	https://github.com/decandia/subsampling
scipy.stats.linregress	SciPy.org	https://docs.scipy.org/doc/scipy/reference/generated/scipy.stats.linregress.html

METHOD DETAILS

All the results are obtained using two stochastic models: (1) Branching Process and (2) (2+1)D Directed Percolation.

Branching Process

We simulate a fully connected (all-to-all) network of $N = 2^{24} \cong 1.6{\cdot}10^7$ nodes that can be in two states, active and quiescent.

1. Starting from the absorbing state, in which all nodes are quiescent, we randomly chose one to activate and start a new avalanche.
2. At each time step $t \to t + 1$ every active site tries to activate every other with probability σ/N where the branching ratio σ is set to the critical value 1.
3. When the total activity $V(t)$ returns to zero, the system is in an absorbing state. A new avalanche is initiated after two steps of quiescence, by activating a new single random site. This restart rule is identical for every avalanche, ensuring statistical stationarity.
4. Subsampling is implemented by fixing a subset of the network $f = N/N_{sub} = 1, 4, 16, 64, 256, 1024$.
5. The simulation ends once $6{\cdot}10^7$ are observed.

(2+1)D directed percolation

We simulate a (2+1)D Directed Percolation of size $L = 1024$, so $N = L^2 = 1048576$ sites.

1. The lattice is first placed in the absorbing state (all sites inactive). An avalanche is triggered by activating a single randomly chosen site at time step $t = 0$. When the activity ends completely, a new seed is placed with the same rule. This guarantees the stationarity of the process. The simulation ends once 10^7 avalanches have been observed.
2. At each time step $t \to t + 1$, every active site attempts to activate its four nearest neighbors with critical probability $p = p_c = 0.28729$. A site remains active for a single time step and then automatically deactivates, becoming susceptible to reactivation in the next time step.
3. We applied spatial sampling in order to select only a subset of the active sites from the entire avalanche propagating through the full lattice. The sites were selected according to a criterion designed to reduce the population size by a factor of $f = \frac{N}{N_{sub}} = 1, 4, 16, 64, 256, 1024$. Note that the case $f = 1$ corresponds to the full lattice case since $N = N_{sub}$.
4. We then implemented temporal coarse graining by aggregating successive time steps into bins of size $\omega = 2, 4, 8, 16, 32,$ and 64. Active sites selected through spatial subsampling and belonging to different time steps were summed within each bin to form a coarse-grained time series. To ensure that only distinct avalanches are considered, a waiting period of $2{\cdot}\omega$ time steps was introduced before initializing a new avalanche.

QUANTIFICATION AND STATISTICAL ANALYSIS

All simulations were run in C++ on the LXGRIV cluster at INFN-Naples. At each time step the code records the number of active lattice sites, which defines the system's activity. An avalanche starts as soon as this count becomes non-zero and ends at the first step in which it returns to zero, as described in the previous section. The time-integrated activity defines the size S, while the number of steps enclosed between start and end defines the duration T. Sizes and durations are binned into logarithmically spaced intervals; counts are then normalized by the total number of avalanches and by the linear width of each bin, yielding the probability densities $P(S)$ and $P(T)$. By summing the sizes of all avalanches that fall into the same duration bin and dividing by the corresponding counts, the code also produces $\langle S(T) \rangle$. These three distributions are shown in the scaling panels (Figures 1A, 1C, 1E, and 4A–4C).

From the same activity trace we extract long-range correlation. Blocks of 2^{14} samples are detrended (mean removal and Bartlett window) and transformed with a real FFT; the resulting powers are grouped into logarithmic bins to build the power spectrum $P(\omega)$, from which the exponent β is estimated (Figures 2A, 2C, 4D, and 5A). In parallel, detrended-fluctuation analysis (DFA) computes the root-mean-square fluctuation *F(n)* over window lengths ranging from 2^2 to 2^{13} samples, and the slope of the log–log plot provides the exponent α.

Exponent estimation follows two separate paths. For the **branching process** the time series shown in Figures 1B, 1D, 1F, 2B, 2D, and 2F is obtained directly as the logarithmic derivative $d \log f(x)/d \log x = \alpha$, of the function $f(x) \propto x^{\alpha}$ during data collection so that the evolution of the exponent can be monitored in real time. For **directed percolation** the analysis is performed in Python (NumPy + SciPy): after importing the distributions saved by the code, the log–log region displaying clear power-law behavior is isolated and a linear fit is carried out with **scipy.stats.linregress**, yielding both the slope (exponent) and its standard error (Figures 5 and 6).

All simulation details are provided in: https://github.com/decandia/subsampling.